MARS
The International Journal of Mars Science and Exploration

MARS INFORMATICS
Open Access Journals

Technology

The Mars Orbiter Laser Altimeter dataset: Limitations and improvements

Sanjoy M. Som[1,2], Harvey M. Greenberg[1] and David R. Montgomery[1,2]

[1]*Dept. of Earth and Space Sciences and Quaternary Research Center,* [2]*Astrobiology Program, University of Washington, Seattle, WA, 98195, USA,* *sanjoy@u.washington.edu*

Citation: Mars 4, 14-26, 2008; doi:10.1555/mars.2008.0002
History: Submitted: April 20, 2007; Reviewed: October 17, 2007; Revised: April 4, 2008; Accepted: April 22, 2008; Published: June 11, 2008
Editor: Oded Aharonson, California Institute of Technology
Reviewers: Oded Aharonson, California Institute of Technology; Patrick McGovern, Lunar and Planetary Institute, Universities Space Research Association

Abstract

Background: The Mars Orbiter Laser Altimeter (MOLA), part of the instrument suite onboard the Mars Global Surveyor spacecraft (MGS), mapped Martian topography between 1999 and 2001. The latest sub-polar dataset, released in 2003, is a 128 pixel per degree digital elevation model (DEM) of the planet, from –87° to +87°. Due to the orbital characteristics of MGS, the resolution is latitude-dependent, being highest near the poles.

Method: We analyze the longitudinal dependence in MOLA data density and find that only a third of the DEM elevation information at the equator comes from raw measurements, the rest being interpolated. Without questioning the enormous scientific value of this dataset, we investigate its limitations qualitatively and quantitatively. We also re-interpolate the dataset using a natural-neighbor with bias scheme that is shown to reduce interpolation-induced errors, particularly for small-scale, East-West trending geomorphic features.

Conclusion: We find that interpolation, especially at the equator, leads to topographical artifacts and smoothing of the terrain that should be appreciated in interpreting geomorphic features that have length scales on the order of the spacing between the orbital tracks that overlap the terrain of interest. Our new interpolation scheme is biased in the East-West direction, improving the overall quality of the elevation model.

Introduction

The Mars Orbiter Laser Altimeter (MOLA) (Zuber et al. 1992), one of five instruments onboard the Mars Global Surveyor (MGS) spacecraft, began mapping the planet in September 1999 (Smith et al. 2001). With a pulse repetition rate of 10 Hz, the laser successfully ranged the planet until the failure of a critical component in June 2001 interrupted the laser trigger. While operational, the instrument surpassed all goals set by the MOLA investigation. It fired over 670 million times (each laser firing is called a "shot"), and generated nearly 9500 orbital profiles, exceeding engineering design limits (Smith et al. 1999). Unlike current airborne LIDAR instruments, MOLA did not scan from side to side in the latitudes between -87° and +87°, the latitudes of interest in this paper (though it was aimed off-nadir to capture polar topography). As such, data was only collected along the orbital track of MGS. The MOLA instrument was capable of 37.5 cm range resolution but due to radial-orbit error, the vertical accuracy obtained was ~1 m when ranging a flat surface (slope <2°). When the instrument ranged terrain with mean slopes greater than 2°, the vertical precision was comparable to 10% of the elevation change within the 168 m in diameter footprint (Smith et al. 2001), although most of the energy may have come from an area as small as 75 m in diameter (Smith et al. 1999). The 10 Hz frequency of the laser-firing limited the along-track spacing between shots to ~300 m (Smith et al. 1999, Smith et al. 2001).

MOLA doesn't measure elevation directly. Rather, it calculates the range to the surface by measuring the time-of-flight of individual laser pulses. This range is subtracted from the spacecraft's orbit location to obtain the planetary radius R_{Mars}. Elevation h is obtained by subtracting the areoid radius R_{areoid} from the planetary radius (Smith et al. 2001). The areoid is defined as representing the surface potential

measured at the mean equatorial radius (3396 km) (Smith et al. 1999).

The MOLA instrument has been used extensively by the scientific community as an aid in understanding the geology, geophysics and geomorphology of the planet, and specifically permitted significant progress in topics as diverse as stratigraphy (Fueten et al. 2005), volcanism (Schultz et al. 2004), atmospheric science (Neumann et al. 1999), surface roughness (Neumann et al. 2003), past transport of water (Williams and Phillips 2001), and internal structure (Zuber 2001). For a summary of MOLA scientific achievements, see Smith et al. 2001.

In May 2003, the latest sub-polar MOLA DEM was released (version L) with a resolution of 128 pixel per degree (ppd), while polar DEMs with resolution as high as 512 ppd were released one year later. In the current work, we will restrict ourselves to the sub-polar 128 ppd DEM, which extends from –87° to +87° latitude. The cartographic projection frame used in the MOLA DEM is the IAU2000 sphere for Mars (Seidelmann et al. 2002).

DEMs are displayed as shaded-relief maps, which are models of how the topography would appear under NW illumination ignoring albedo. A raster DEM is a regular grid of points, each with discrete information on elevation. The MOLA DEM grid points that did not stem from a direct elevation measurement by MOLA were interpolated using a minimum-curvature-under-tension (MCUT) scheme (Smith et al. 2001; Smith and Wessel 1990). The Generic Mapping Tool (GMT) software (Wessel and Smith 1991) was used for the interpolation since it contains a built-in MCUT algorithm with a user selectable tension parameter (*T*). A tension parameter of 0.5 was used in the creation of the currently available MOLA DEM.

As in most interpolation schemes, artifacts introduced in the dataset may skew data analysis in studies involving the resulting DEMs. We first evaluate the MOLA DEM resolution to assess potential interpretive pitfalls and errors caused by artifacts and smoothing. We then inspect different interpolation schemes, and introduce a new DEM for Mars, UWMOLA, based on a natural-neighbor-with-bias (NNB) scheme.

Nature of the 2003 MOLA DEM

MOLA datasets are available from the NASA Planetary Data System (PDS), and can be found at different stages of processing leading to the DEM. MGS's orbital inclination of 93° permitted MOLA to obtain nadir measurements of the mid-latitudes from -87° to +87°. Data, once sent by the spacecraft and received through the Deep Space Network (DSN) in binary packages, were assembled into Aggregated Experiment Data Records (AEDRs). The AEDRs were then processed for errors (such as non-nadir pointing, errors in calibration and spacecraft location…) yielding Precision Experiment Data Records (PEDRs). PEDRs incorporate the areoid and as such, elevation information is directly available from them (Smith et al. 1999). PEDRs also include altimetric cross-over correction. Altimetric cross-overs are the difference in radial distance measured at a common location from two distinct intersecting ground tracks (Neumann et al. 2001). A cross-over analysis allows for better estimates of the spacecraft's position during ranging, since tracking from DSN is discontinuous. Indeed, following correction, position is known within <100 m, which is less than a shot footprint (168 m in diameter), and elevation is known to within <1 m (Neumann et al. 2001).

With data from PEDRs, Experiment Gridded Data Records (EGDRs) are created. Initial Experiment Gridded Data Records (IEGDRs), which encompass at least the first 30 days of the mission, and Mission Experiment Data Records (MEGDRs) consisting of data up to when the instrument stopped working, are created from the EGDRs.

The MEGDRs are the DEMs, and come from the interpolation of the PEDRs. They are gridded at several resolutions: 4, 16, 32, 64 and 128 ppd for the mid-latitudes (up to ±87°) (Smith et al. 2003). In addition to the information included in PEDRs, MEGDRs also contain the number of shots per grid cell. For clarification, a *grid cell* is the basic unit of composition of a dataset, which may contain several types of information for that particular unit (elevation, number of shots etc…), however, what is displayed on the DEM is a *pixel* (picture element), which is the grid-cell information displayed for a particular attribute, such as elevation. With a shot footprint of 168 m in diameter, the number of shots per grid cell will decrease with increasing resolution, since the 4 ppd DEM has a grid cell dimension (width scales with the cosine of the latitude) of ~14.8 km, whereas the 128 ppd has a grid cell size of ~460 m.

Analysis

Latitude-dependent resolution

The frequency of the number of shots per grid cell varies significantly for the different resolution MOLA DEMs (Figure 1). Because the laser fired at regular intervals, the number of shots per cell scales with grid cell size. For the 128 ppd DEM, most grid cells are devoid of shots (Figure 1c), which indicates that data for the majority of the cells are generated by interpolation. Figure 1d illustrates how track spacing generates peaks in the frequency diagram in, for example, Fig 1b. In addition, the percentage of grid cells

Table 1. Percent coverage and pixel length scale for available MOLA DEMs between –60° and +60° latitude

DEM [pixel per degree]	Pixel length scale [km]	Coverage [% of cells containing ≥ 1 shot]
4	14.82	100
16	3.71	96
32	1.85	81
64	0.93	55
128	0.46	31

containing shots is both latitude and scale dependent (Figure 2). Just 31% of the grid cells between –60° and +60° latitude contain an actual elevation measurement for the 128 ppd DEM. The elevation values of two-thirds of the grid cells in the highest resolution DEM, the most appropriate for geological and geophysical studies, are thus interpolated. This coverage increases, however, to 100% for the 4 ppd DEM (Table 1).

Interpolation-caused artifacts and smoothing

The interpolation provided by the MCUT algorithm creates the potential for geomorphic misinterpretations, especially for high-frequency, low amplitude topographical features, which are often "drowned" in the large MOLA spacing and interpolation-caused smoothing of the DEM (see Beyer and McEwen 2005, Figure 8). Features that fall into "MOLA gaps" (Figure 4) between widely-spaced tracks will be lost, and long and narrow features such as valleys, faults and grabens, are prone to being deformed (Figure 3) as they cross these data gaps.

Discussion

Interpolation technique used to create the DEMs

The discrete data points in the PEDRs were interpolated to form a continuous surface DEM using the MCUT algorithm (Smith et al. 2001; Smith and Wessel 1990) and distributed as MEGDRs. The interpolation was performed using the *surface* routine built in the Global Mapping Tools (GMT) software v3.4.3. To avoid high-frequency elevation changes along track within the final DEM (Okubo et al. 2004), the data were pre-filtered to ensure that no information was contained at wavelengths shorter than twice the grid spacing

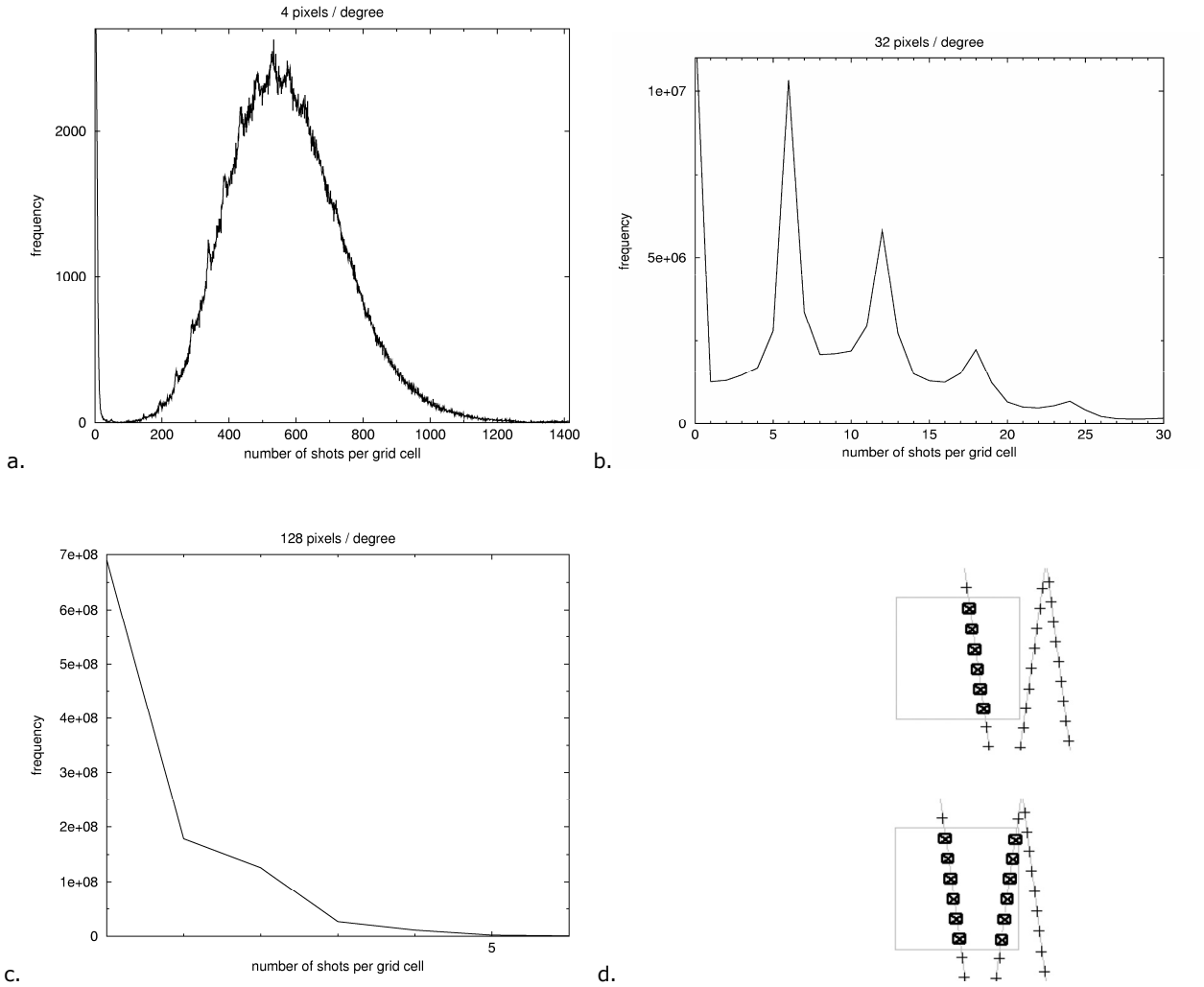

Figure 1. Frequency of grid cells for Mars MOLA DEMs having a given number of shots: **(a)** 4 ppd (figure1a.png), **(b)** 32 ppd (figure1b.png), **(c)** 128 ppd (figure1c.png), **(d)** illustrates how orbital geometry and spacing leads to the period peaks, which are seen especially in graph (b). The light square represents a grid cell and the bold crossed small boxes represent data points located on orbital tracks. Top image is for the peak at x = 6 in (b), and bottom image is for the peak at x = 12 in (b). (figure1d.png).

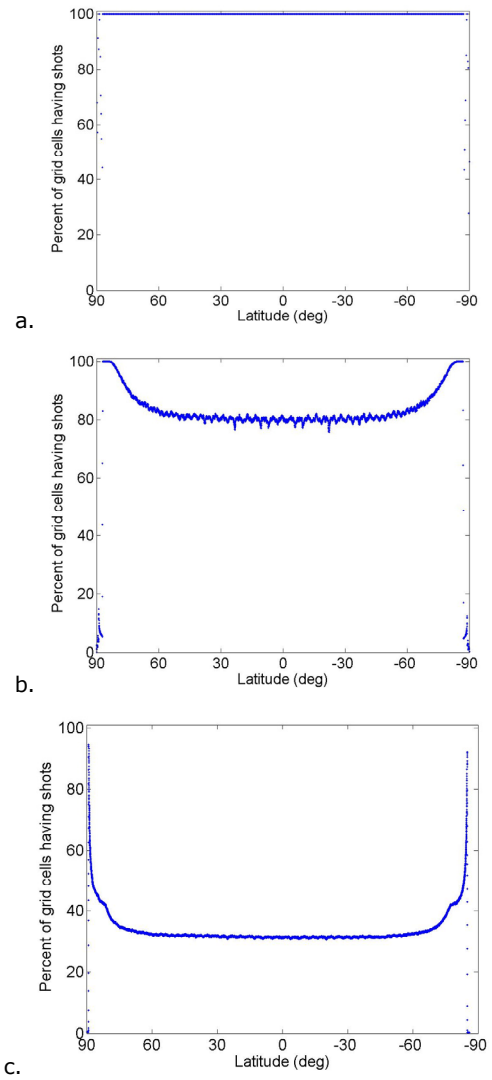

Figure 2. Latitudinal variation in the percent of MOLA DEM grid cells having ≥ 1 shot: **(a)** 4 ppd (figure2a.png), **(b)** 32 ppd (figure2b.png), **(c)** 128 ppd (figure2c.png). Resolution actually improves more rapidly with latitude because grid cells are smaller as one approaches the poles.

(Smith and Wessel 1990). Okubo et al. 2004 studied the DEM integrity by using GMT and found that the *surface* routine, independent of the choice of filtering routines, produced the lowest elevation difference compared with the original PEDR "regardless of the surface-specific interpolation option used", implying that changing tension did not improve the interpolation to any significant degree. Given their comparison method to the raw PEDR data, this is not surprising. The minimum-curvature routine is a natural bicubic spline that forces the interpolation function to pass through the data points exactly. Furthermore, it is formulated such that the squared curvature integrated over the entire surface is minimized (Smith and Wessel 1990). Adding tension will change the behavior of the function *between* data points, but the function will still remain "pinned" to the data points. By adding tension, the requirement that the total curvature be minimized is relaxed, and unwanted oscillatory behavior yielding inflexion points between the data points is removed (Smith and Wessel 1990). Although we recognize the minimum-curvature under tension oxymoron (since with tension, the curvature will no longer be minimum), we choose to leave the syntax untouched, since the algorithm has been described as such in the MOLA literature. Adding tension is analogous to pulling uniformly along the edges of an elastic sheet (the surface function) fitted over the data points.

Abramov and McEwen (2004) compared *minimum-curvature* (without tension), *nearest neighbor*, *natural neighbor* and *linear interpolation* routines. Their findings, based on qualitative and quantitative analysis, suggest that the natural neighbor interpolation routine (Sambridge et al. 1995; Sibson 1980) is superior to the other three, in that visual artifacts are minimized. Rather than comparing with the raw PEDR data, their quantitative analysis was performed by overlapping a random MOLA-sized track grid above a higher resolution DEM of a region in Iceland. Only the elevation data below the tracks were recorded, simulating MOLA sampling. From these elevation data, new DEMs, using all four interpolation routines, were created. The original Iceland DEM was then subtracted from the simulated MOLA DEM of Iceland. They found that the natural neighbor routine, in addition to producing the best qualitative DEM, produced the overall lowest mean topography difference between the high-resolution DEM and the interpolated one. They conclude, similar to Slavney, that minimum-curvature should only be used for a "quick first-order interpolation" (Abramov and McEwen 2004).

The natural neighbor algorithm and its tuning with horizontal bias

It is useful at this stage to clearly distinguish between *data* points, which are the location of each elevation measurement (shots) along orbital tracks, and *grid* points (located at the center of the respective grid cells), which are the loci of points forming the artificial grid upon which the DEM is calculated.

The natural neighbor algorithm is ideally suited for gridding and interpolating irregularly spaced data (Sambridge et al. 1995), making it ideal for the Martian dataset. In our application, it inputs elevation data points along MGS's orbital tracks, and outputs the interpolated grid elevations, forming the DEM.

As illustrated in Figure 5a, the algorithm first grids the MOLA data points into a Voronoi diagram, which is a combination of Voronoi cells (or Thiessen polygons). Each Voronoi cell about a data point represents the loci of areas that are closest to it. Next, each grid cell is interpolated based on the influence of its "natural neighbors". This is shown in Figure 5b for six representative grid points (boxed crosses). The bold lines show the Voronoi cells of the data points and the 6 grid points. The Voronoi cell of each data point that is intersected by the Voronoi cell of a grid point is a natural

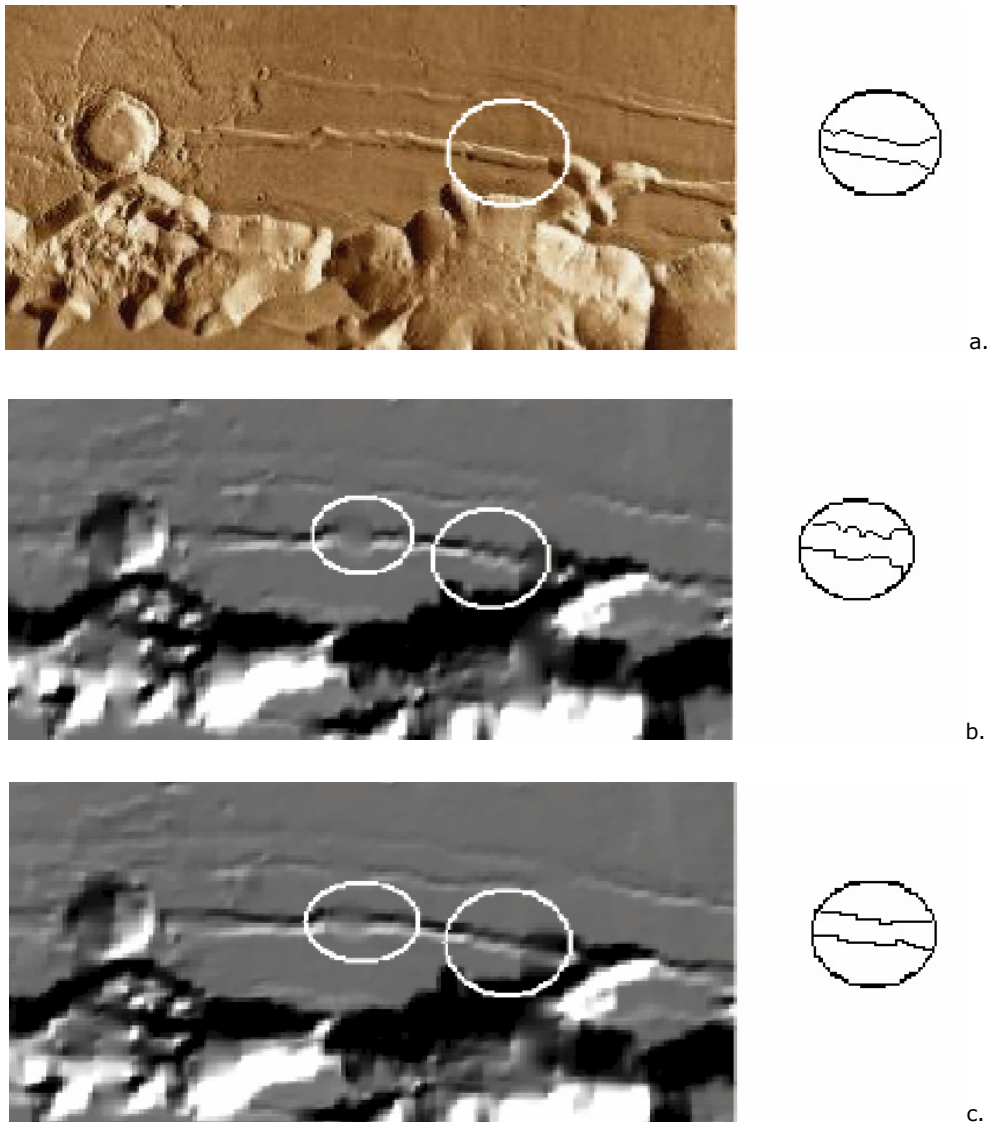

Figure 3. Example of East-West terrain deformation and smoothing due to interpolation (center of circle: 278.05E – 4.48N). **(a)** THEMIS IR (Christensen et al. 1996) (figure3a.png). **(b)** MOLA MCUT DEM (figure3b.png). **(c)** NNB1.5X DEM (figure3c.png). The large circles are represented on the right with an outline of the linear feature's rim, and are an example of deformation. The small circles show artifacts of terrain smoothing.

neighbor of that grid point, and contributes to the final interpolated elevation value at that grid point. Its contributing weight is proportional to the area of its Voronoi cell that overlaps the Voronoi cell of the grid point. This is the first important property of the natural neighbor algorithm. In practice, the Voronoi cell and its associated weights are calculated independently for each grid cell. The second property is a direct consequence of the first. The natural neighbor algorithm is a local procedure, since there are only a limited number of data points that influence the value of a particular grid point.

Figure 5c is similar to Figure 5a, but the grid and data points were "squeezed" or biased in the X dimension by dividing the X-coordinates of the data points by a factor *m* (varied in the range 1.5 - 3) before running the interpolation scheme. This was done since across-track spacing is usually much larger than the interval between shots along-track, causing MOLA holes. Figure 5d is the analog of 5b, but created with biased data. As a result of the bias, grid cells are more closely associated with their neighbors to the left and right, rather than above and below. This yields improved East-West interpolation, without significantly sacrificing North-South accuracy, since the data points already have a North-South trend. The last important property is that the interpolated function is continuously differentiable at all points except at the grid cell (Sambridge et al. 1995).

Following the conclusions of Abramov and McEwen (2004), we re-interpolated the MOLA PEDRs using the natural

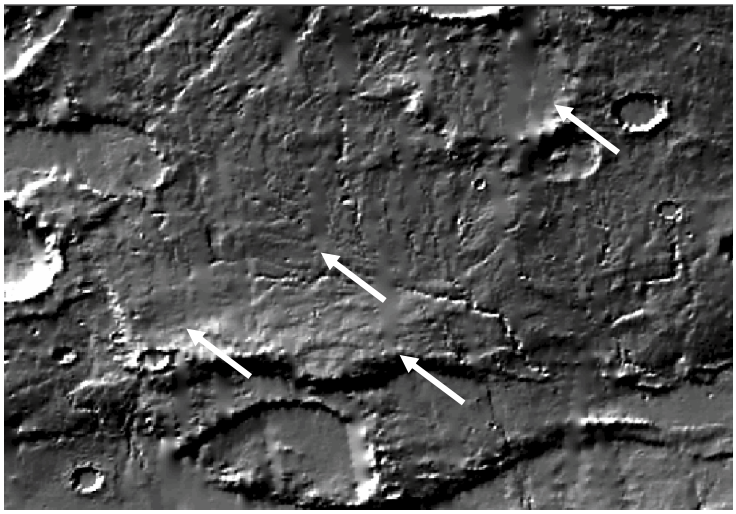

a.

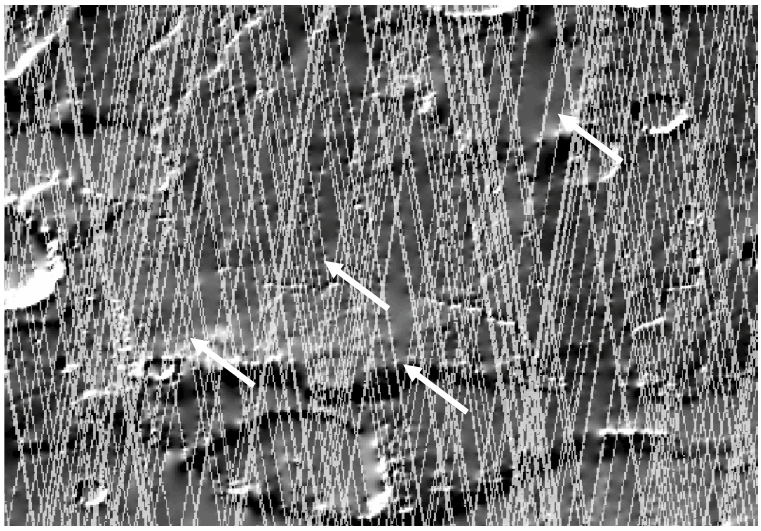

b.

Figure 4. Example of a "MOLA gap" on the shaded relief map of Warrego Vallis (267.5E, -42.3N). **(a)** Shaded relief map (figure4a.png). **(b)** Shaded relief map with orbital tracks (figure4b.png). Major gaps arrowed.

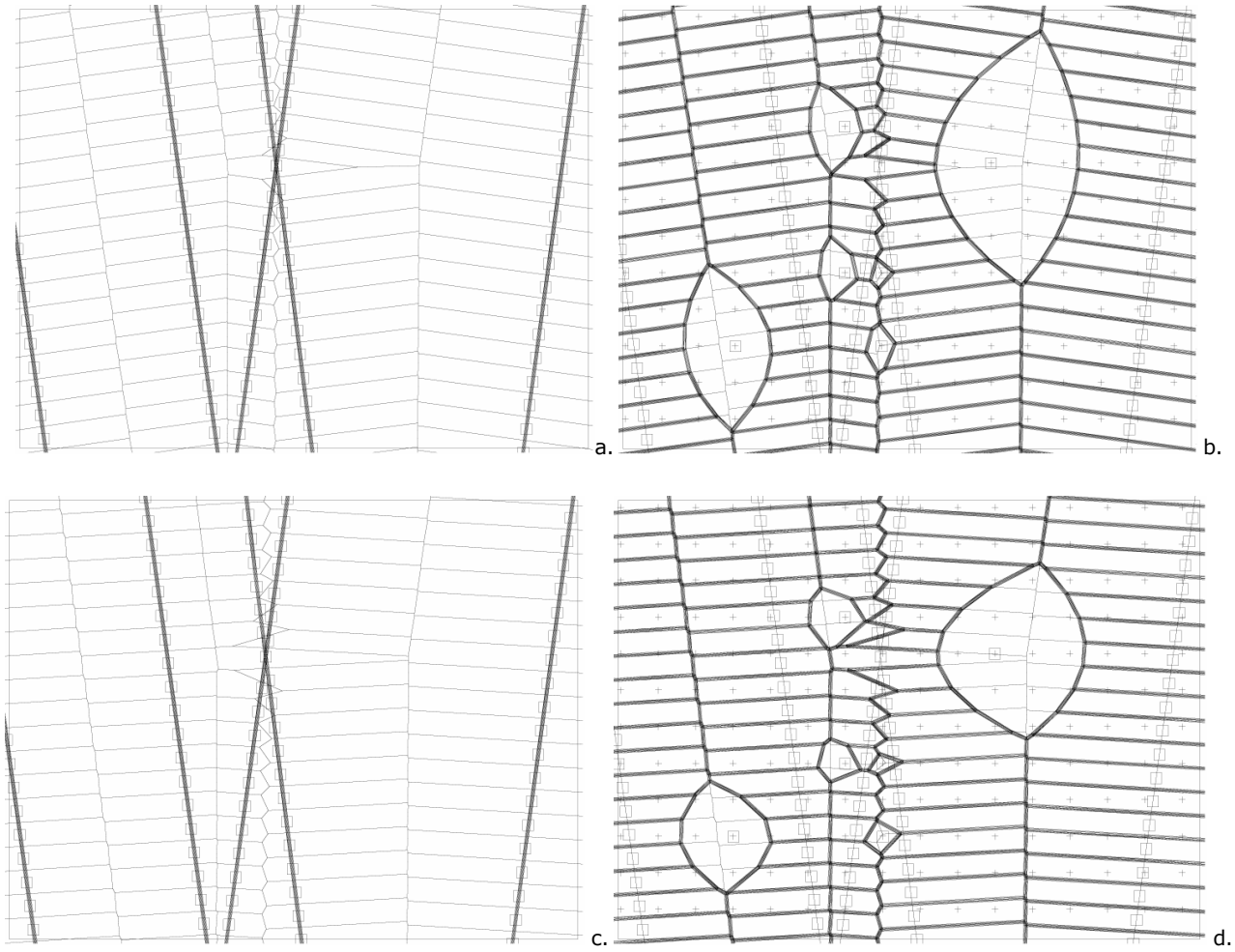

Figure 5. (a) MOLA tracks, data points and grid points with respective Voronoi cells (MCUT) (figure5a.png). **(b)** Voronoi cells of 6 representative points (MCUT) (figure5b.png). **(c)** Same as (a) but for NNB1.5X (figure5c.png). **(d)** Same as (b) bur for NNB1.5X (figure5d.png). See text for details.

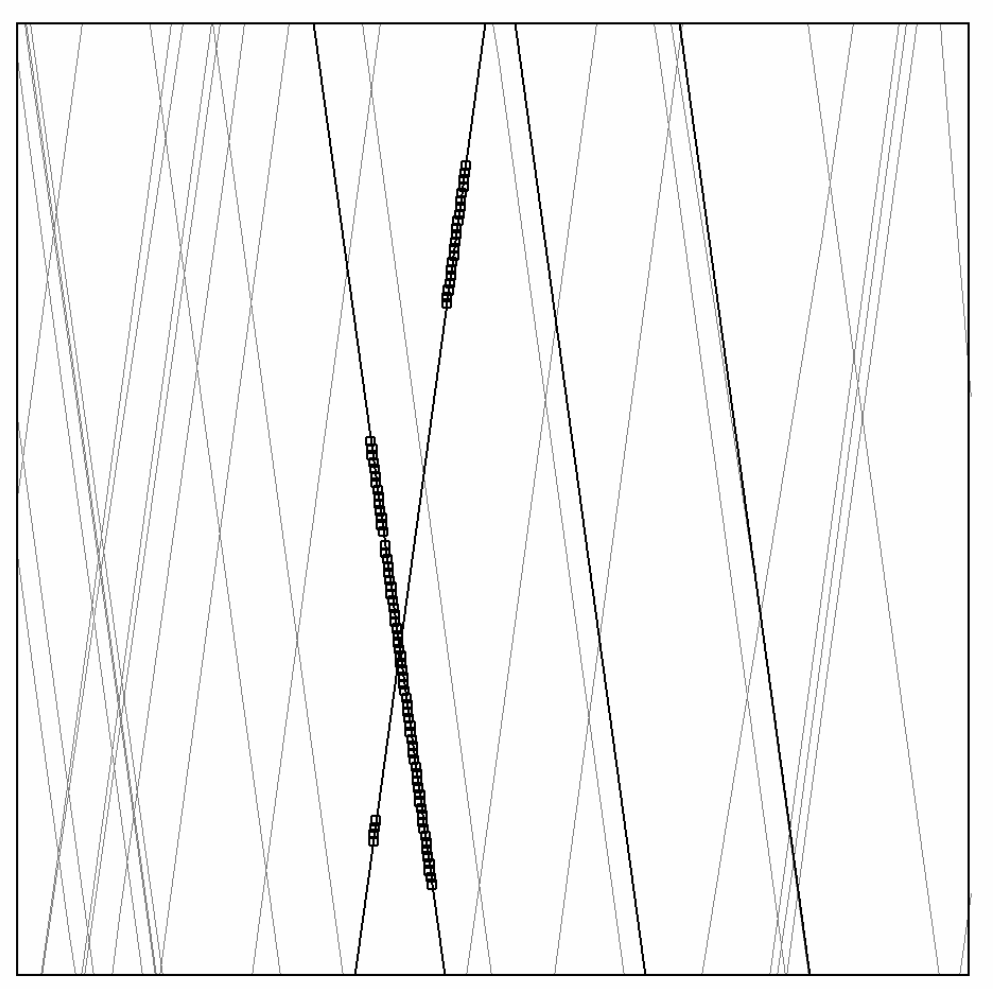

Figure 6. Incorporating data points on poorly calibrated tracks that are otherwise removed. Gray lines represent the "good" well-calibrated MOLA tracks, bold lines represent removed "bad" tracks, and the boxes represent data points on the removed tracks that are more that 0.03^{o} from any good point and have thus been re-inserted in the locus of points used for interpolation (figure6.png).

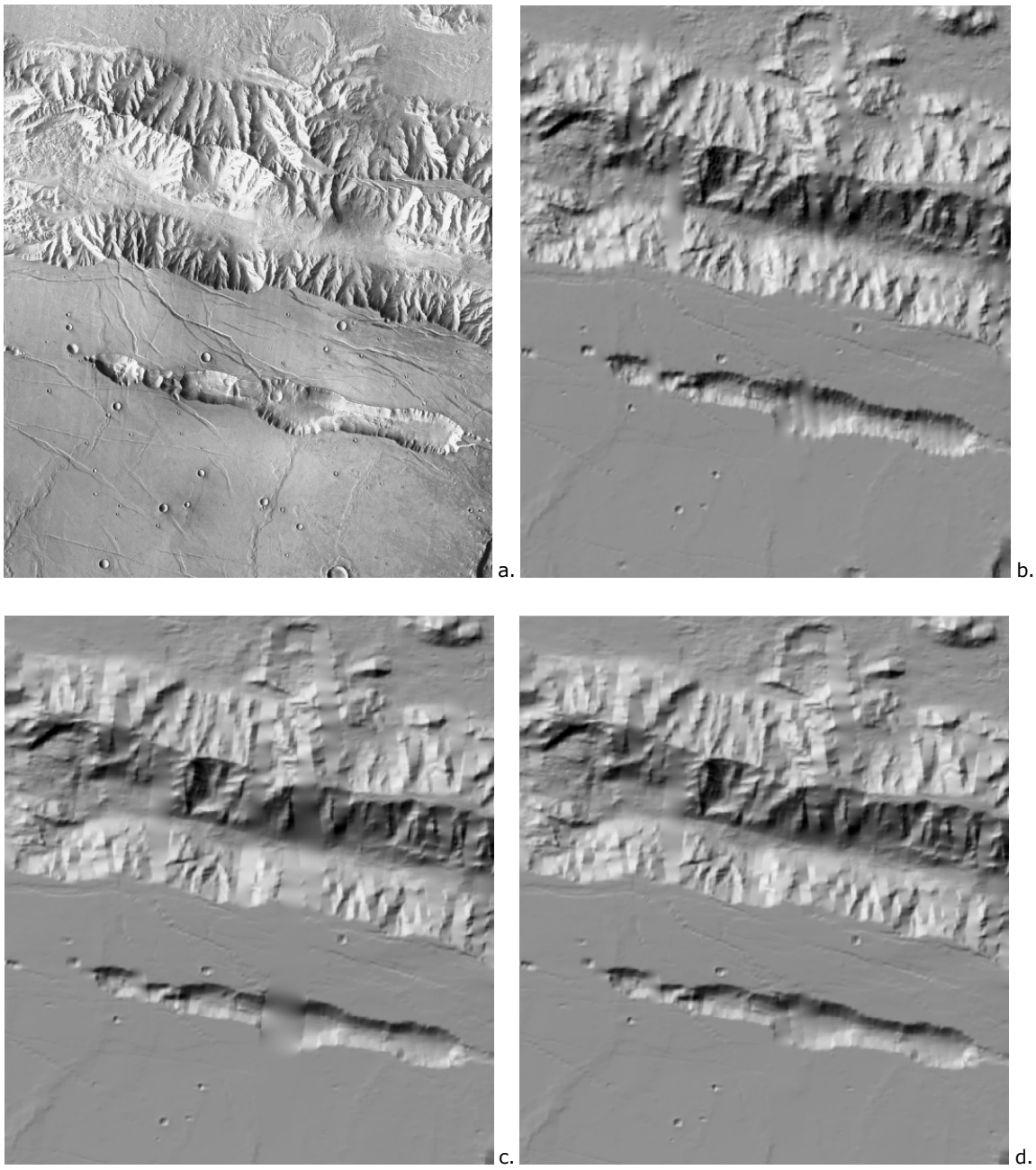

Figure 7. Application of Figure 6: Effect of re-inserting data points on poorly calibrated MOLA tracks that are more than 0.3° away from a good point. **(a)** THEMIS mosaic (Christensen et al. 2006) (figure7a.png). **(b)** Standard DEM (figure7b.png). **(c)** Natural Neighbor with 1.5X bias with bad tracks omitted (figure7c.png). **(d)** Natural Neighbor with 1.5X bias with suspicious points restored (see text for details) (figure7d.png). The ~140 km long "graben" is located at –15N, 294E.

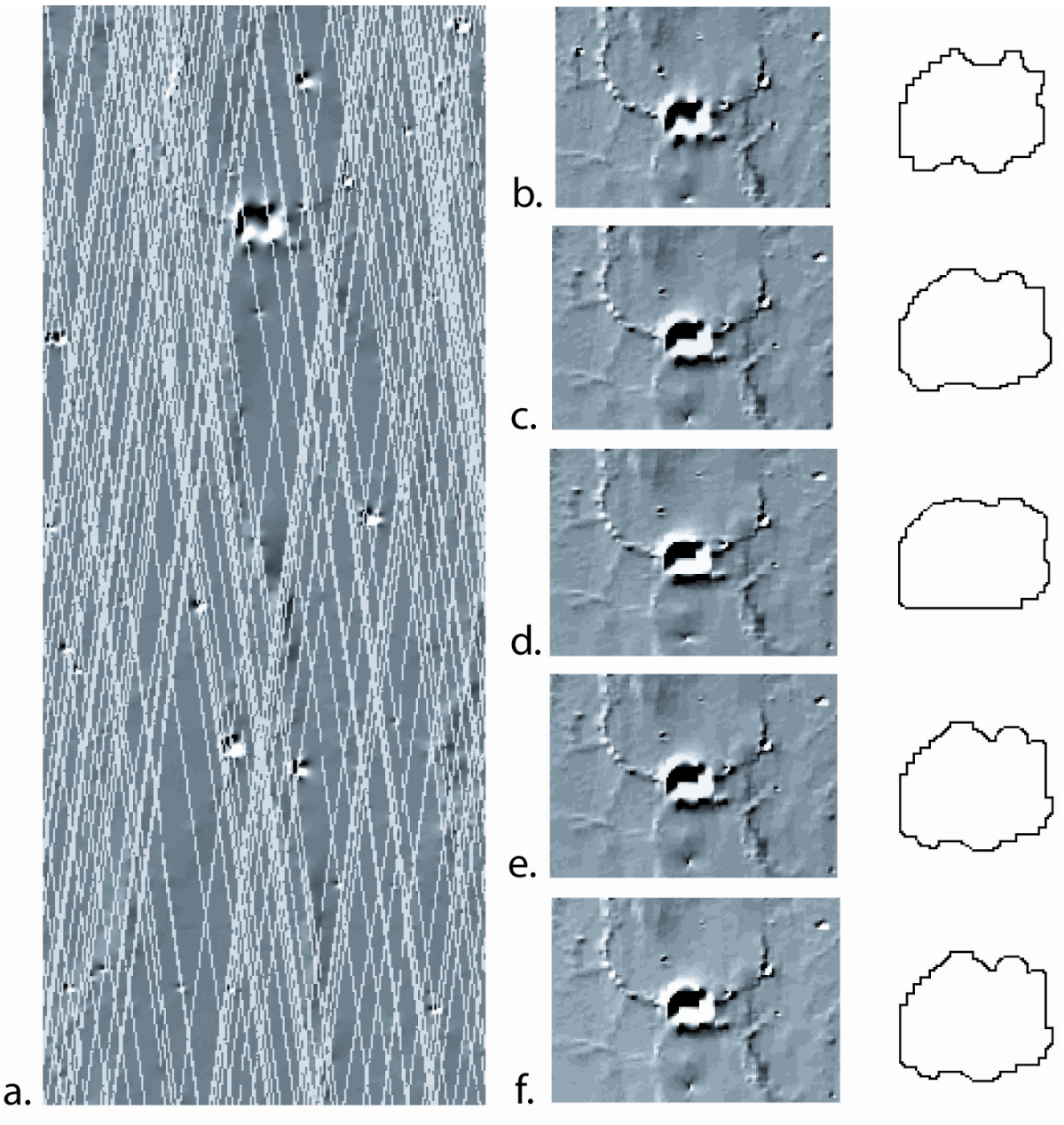

Figure 8. Shaded relief map of South West of Bahram Vallis with MGS orbital tracks. **(a)** Arrowed crater is 12km wide and is located in a MOLA hole (299.1E, 18.5N). **(b)** MCUT, **(c)** Natural Neighbor, **(d)** Natural Neighbor with 1.5X bias, **(e)** Natural Neighbor with 2X bias, **(f)** Natural Neighbor with 3X bias. Sun is at a 35° elevation to the NW, the rim of crater is depicted on the right (figure8.png).

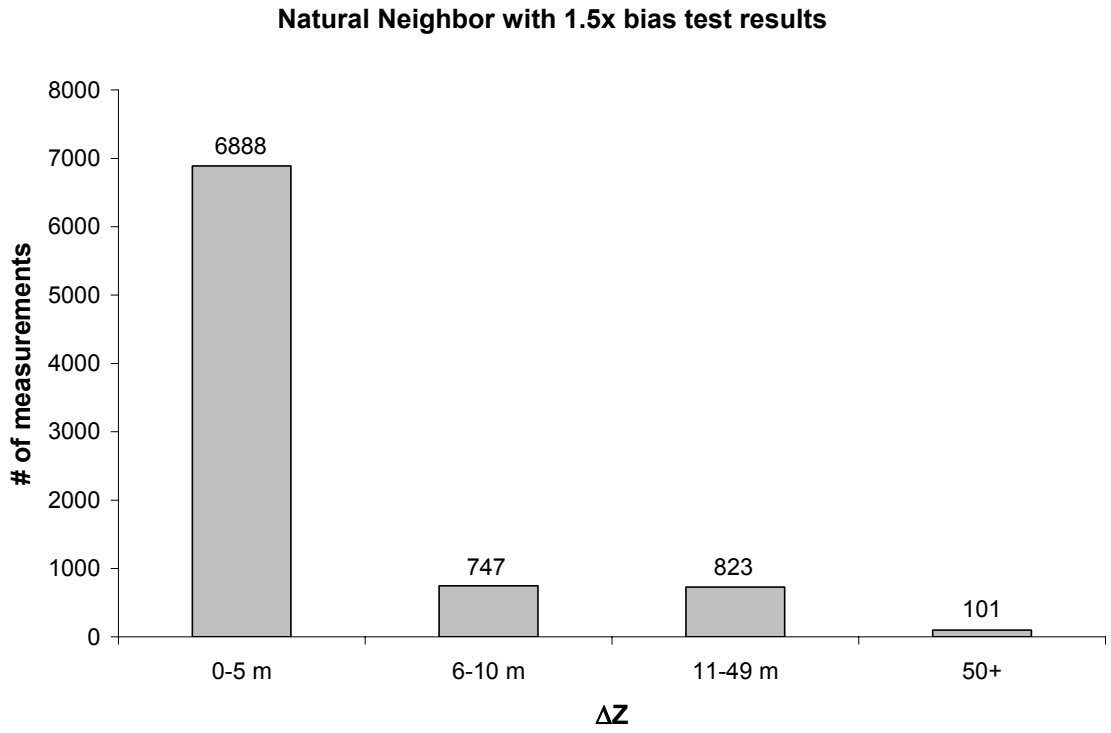

Figure 9. Binning of 8466 ΔZ values, defined as the difference between 8466 actual PEDR elevation measurements in a random 4° x 4° tile, and the interpolated values at the same location, but with those PEDR data removed (figure9.png).

neighbor interpolation routine *Natgrid*, part of the *ngmath* library built into NCAR Graphics. In addition to the biasing described above, erroneous PEDR tracks were removed to avoid the incorporation of linear artifacts in the DEM. Howard provided an additional list of erroneous tracks, compiled by comparing the differences between elevations from those tracks with the average elevations obtained from other tracks, discarding those found to be strongly biased. However, in areas where the data points along those erroneous tracks were more than 0.03° away from the nearest good point (Figure 6), those points were kept, since they provided better data than no data at all (Figure 7).

We compared natural neighbor and natural neighbor with *m*X bias both qualitatively and quantitatively. Figures 3b,c, 7 and 8 show how adding a 1.5X bias improves East-West features the best: irregularities in quasi-linear features caused by the MCUT algorithm, such as crater rim or canyon walls, are removed using NNB, making the DEM more consistent with the actual morphology.

A random 4° x 4° tile of PEDR data was chosen to quantitatively study the effect of biasing on the resulting DEMs. Our test methodology involved removing orbital tracks, re-interpolating the data, and comparing the original PEDR elevation values with those obtained from the newly created DEMs. More specifically, we removed 11 non-interacting tracks and created several DEMs using the natural neighbor scheme with different biases. Next, elevation data at the coordinates of PEDR data points were then interpolated using the nearest four MOLA DEM grid points, by applying a bilinear scheme (since a DEM grid point did not necessarily coincide with a PEDR data point). The two values were then subtracted creating a new value ΔZ. From those eleven tracks, 8466 ΔZ measurements were obtained, and binned into 4 categories: $0 \leq \Delta Z \leq 5$ m, $5 < \Delta Z \leq 10$ m, $10 < \Delta Z < 50$ m and $\Delta Z > 50$ m. This was done for biases of 1x, 1.5x, 2x and 3x. The best result, defined as the most measurements grouped in the smallest bins, was found to be 1.5x and is shown in Figure 9. In addition to being the best algorithm based on qualitative interpretation (Figure 7), the bias of 1.5x also proved superior to the other biases in this quantitative test.

The NNB algorithm is particularly well suited for improving the representation of East-West trending geomorphic features, compared with the standard MCUT algorithm, as we have seen. However, in terrain lacking such features, or where such features are not dominant, the NNB algorithm was not found to provide discernable advantage. As such, we recommend the NNB1.5X mainly for small scale, dominantly East-West trending features, and particularly for such features that approach the limit of the DEM grid size. Generally, features within large MOLA gaps should be studied through imagery or through custom DEMs built from stereo pairs.

Re-interpolation of PEDR data

Encouraged by the several test cases presented in this paper

we re-interpolated the PEDR data between -60° and +60°, and are making the new DEM freely available to the research community. To do this, we cropped the data into 4° square tiles (with an added 0.25° margin), omitting data points from suspect orbital tracks, as well as points that were individually tagged as suspect (but adding back suspect data points in the middle of large data gaps), and using a false origin to maintain full precision with 32-bit floats. We used a bias equal to 1.5 multiplied by a correction factor of *cos*(latitude). A small C wrapper program read the data and divided the X coordinates and the output cell width by the bias factor before passing the data to the *Natgrid* subroutine for gridding. The data was then imported into a GIS environment (with workarounds for signed integers) where decompression was accomplished when the biased cells from *Natgrid* were interpreted as square cells in the GIS. The new DEM (UWMOLA), a 128 ppd dataset interpolated using the 1.5X NNB algorithm, is being added to the GIS data web-served by the Geomorphological Research Group at the University of Washington.

In this paper, we reviewed the process of obtaining the MOLA DEMs, and evaluated their latitude dependent nominal resolution. We found that between –60 and +60 degrees of latitude, the latest MOLA DEM is heavily interpolated and this causes artifacts and smoothing that may affect geomorphic interpretation of terrain. We inspected different interpolation schemes, and presented a new DEM for Mars based on the natural-neighbor-with-bias (NNB) scheme. We found that a 1.5X bias produced the best DEM, although improved representation is primarily apparent in small-scale, dominantly East-West trending geomorphic features.

Directory of Supporting Data

root directory

- som_mars_2008_0002.pdf
  Full-resolution images
  - Fig. 1 figure1a.png, figure1b.png, figure1c.png, figure1d.png
  - Fig. 2 figure2a.png, figure2b.png, figure2c.png
  - Fig. 3 figure3a.png, figure3b.png, figure3c.png
  - Fig. 4 figure4a.png, figure4b.pbg
  - Fig. 5 figure5a.png, figure5b.png, figure5c.png, figure5d.png
  - Fig. 6 figure6.png
  - Fig. 7 figure7a.png, figure7b.png, figure7c.png, figure7d.png
  - Fig. 8 figure8.png
  - Fig. 9 figure9.png

Acknowledgements

We thank Susan Slavney of the MOLA PDS geoscience node for kindly answering our questions, as well as Alan Howard who provided us with a list of erroneous MOLA tracks. Stephen Wood and Gregory Neumann provided useful feedback on our analysis and on an early manuscript. The current manuscript benefited from the reviews of Oded Aharonson and Patrick McGovern.

References

Abramov, O. and A. S. McEwen (2004) "An evaluation of interpolation methods for Mars Orbiter laser Altimeter (MOLA) data" International Journal of Remote Sensing 25, 669-676. doi:10.1080/01431160310001599006

Beyer, R. A. and A. S. McEwen (2005) "Layering stratigraphy of eastern Coprates and northern Capri Chasmata, Mars" Icarus 179, 1-23. doi:10.1016/j.icarus.2005.06.014

Christensen, P. R., N. S. Gorelick, G. L. Mehall and K. C. Murray (2006) "THEMIS Public Data Releases" Planetary Data System node. Arizona State University.

Fueten, F., R. M. Stesky and P. MacKinnon (2005) "Structural attitudes of large scale layering in Valles Marineris, Mars, calculated from Mars Orbiter Laser Altimeter data and Mars Orbiter Camera imagery" Icarus 175, 68-77. doi:10.1016/j.icarus.2004.11.010

Neumann, G. A., D. D. Rowlands, F. G. Lemoine, D. E. Smith and M. T. Zuber (2001) "Crossover analysis of Mars Orbiter Laser Altimeter data" Journal of Geophysical Research 106, 23753-23768. doi:10.1029/2000JE001381

Neumann, G. A., D. E. Smith and M. T. Zuber (1999) "Two Mars years of clouds detected by the Mars Orbiter Laser Altimeter" Journal of Geophysical Research 108, 5023. doi:10.1029/2002JE001849

Neumann, G. A., J. B. Abshire, O. Aharonson, J. B. Garvin, X. Sun and M. T. Zuber (2003) "Mars Orbiter Laser Altimeter pulse width measurements and footprint-scale roughness" Geophysical Research Letters 30, 1561. doi:10.1029/2003GL017048

Okubo, C. H., R. A. Schulz and G. S. Stefanelli (2004) "Gridding Mars Orbiter Laser Altimeter data with GMT: effects of pixel size and interpolation methods on DEM integrity" Computers & Geosciences 30, 59-72. doi:10.1016/j.cageo.2003.10.004

Sambridge, M., J. Braun and H. McQueen (1995) "Geophysical parametrization and interpolation of irregular data using natural neighbors" Geophysical Journal International 122, 837-857. doi:10.1111/j.1365-246X.1995.tb06841.x

Schultz, R. A., C. H. Okubo, C. L. Goudy and S. J. Wilkins (2004) "Igneous dikes on Mars revealed by Mars Orbiter Laser Altimeter topography" Geology 32, 889-892. doi:10.1130/G20548.1

Seidelmann, P. K. et al. (2002) "Report of the IAU/IAG Working Group on cartographic coordinates and rotational elements of the planets and satellites:2000" Celestial Mechanics and Dynamical Astronomy 82, 83-110. doi:10.1023/A:1013939327465

Sibson, R. (1980) "A brief description of natural neighbour interpolation" Looking at Multivariate Data. V. Barnett ed. Wiley 21-36.

Smith, D. E., W. L. Sjogren, G. L. Tyler, G. Balmino, F. G. Lemoine and A. S. Konopliv (1999) "The gravity field of Mars: Results from Mars Global Surveyor" Science 286, 94-97. doi:10.1126/science.286.5437.94

Smith, D. E. et al. (2001) "Mars Orbiter Laser Altimeter: Experiment summary after the first year of global mapping of Mars" Journal of Geophysical Research 106, 23689-23722. doi:10.1029/2000JE001364

Smith, D. G., G. Neumann, R. E. Arvidson, E. A. Guinness and S. Slavney (1999) "Mars Global Surveyor Laser Altimeter Precision Experiment Data Record" NASA Planetary Data System. MGS-M-MOLA-3-PEDR-L1A-V1.0.

Smith, D. G., G. Neumann, R. E. Arvidson, E. A. Guinness

and S. Slavney (2003) "Mars Global Surveyor Laser Altimeter Mission Experiment Gridded Data Record" NASA Planetary Data System. MGS-M-MOLA-5-MEGDR-L3-V1.0.

Smith, W. H. F. and P. Wessel (1990) "Gridding with continuous curvature splines in tension" Geophysics 55, 293-305. doi:10.1190/1.1442837

Wessel, P. and W.H.F. Smith (1991) "Free software helps map and display data" EOS Transaction American Geophysical Union 72, 441,445-446. doi:10.1029/90EO00319

Williams, R. M. E. and R. J. Phillips (2001) "Morphometric measurements of martian valley networks from Mars Orbiter Laser Altimeter (MOLA) data" Journal of Geophysical Research 106, 23737-23751. doi:10.1029/2000JE001409

Zuber, M. T. (2001) "The crust and mantle of Mars" Nature 412, 220-227. doi:10.1038/35084163

Zuber, M. T., D. E. Smith, S. C. Solomon, D. O. Muhleman, J. W. Head, J. B. Garvin, J. B. Abshire and J. L. Bufton (1992) "The Mars Observer laser altimeter investigation" Journal of Geophysical Research 97, 7781-7797.